Electronic Supplementary Material (ESI) for Nanoscale

High-Performance n-Si/α-Fe_2O_3 Core/Shell Nanowire Array Photoanode towards Photoelectrochemical Water Splitting

Xiaopeng Qi,[ab] *Guangwei She,* *[a] *Xing Huang,*[a] *Taiping Zhang,*[a] *Huimin Wang,*[a] *Lixuan Mu,*[a] *and Wensheng Shi**[a]

[a] Key Laboratory of Photochemical Conversion and Optoelectronic Materials, Technical Institute of Physics and Chemistry, Chinese Academy of Sciences, Beijing, 100190, P. R. China

[b] General Research Institute for Nonferrous Metals, Beijing, 100088, China

SEM images of Si nanowires with different lengths

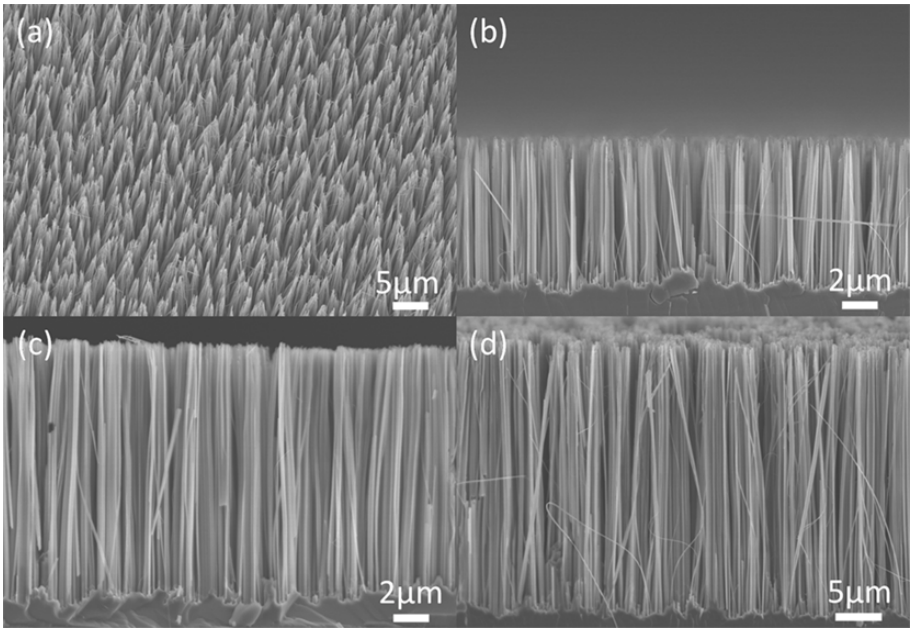

Figure S1. (a) Plan-view SEM images of SiNWs fabricated by a modified Peng's method[1] with an etching time of 20 min; (b), (c) and (d) Side-view SEM images of SiNWs with an etching time of 5 min, 10 min and 20 min.

Additional composition characterization of the n-Si/α-Fe_2O_3 nanowires

The element composition of the n-Si/α-Fe_2O_3 products was analyzed by Energy Dispersive X-ray Spectrum (EDX) and X-ray Photoelectron Spectroscopy (XPS) to investigate the possibilities of any impurities doping, such as possible N incorporation from the $Fe(NO_3)_3$ to the products. As shown in Figure S2a, expect for the signals for Si, Fe, O, and Cu, no other elements were detected in the EDX analysis. The Cu signals came from the Cu grid that we used to support our product. XPS measurement was also performed. As shown in Figure S2b, except for the noise signal, no peaks were detected in the binding energy range of 390-412 eV, where N 1s signals are usually observed.

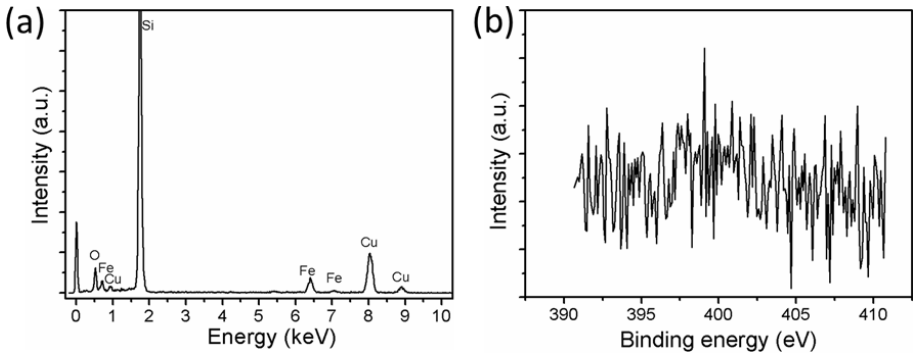

Figure S2. (a) The full EDX spectrum collected from an n-Si/α-Fe_2O_3-20mM sample; (b) The XPS spectrum collected from an n-Si/α-Fe_2O_3-20mM sample in the binding energy range of 390-412 eV, where signals for N 1s are usually located.

Photoelectrochemical characterization of the α-Fe_2O_3 on FTO

Figure S3a shows the linear scan voltammograms (LSVs) of the α-Fe_2O_3 prepared on FTO (α-Fe_2O_3/FTO), in dark and under irradiation. Figure S3b is a SEM image of the as-prepared α-Fe_2O_3, showing that the prepared α-Fe_2O_3 is very smooth and planar. The α-Fe_2O_3/FTO showed much less photoresponse than the n-Si/α-Fe_2O_3 samples, exhibiting a small photocurrent of 12.5 μA/cm^2 at 1.23 V vs RHE and a photocurrent on-set potential of about 0.78 V vs RHE. The small dark current could be attributed to the charging/discharging of the depletion layer of α-Fe_2O_3 as the potential was scanned, as well as the adsorption/disadsorption of ions at the α-Fe_2O_3 surface. This small dark current could also be observed on bare FTO and Pt electrodes. The poor photoelectrochemical performance of the α-Fe_2O_3 should be related to its planar and smooth architecture, which offers minimized area of the α-Fe_2O_3/electrolyte interface.

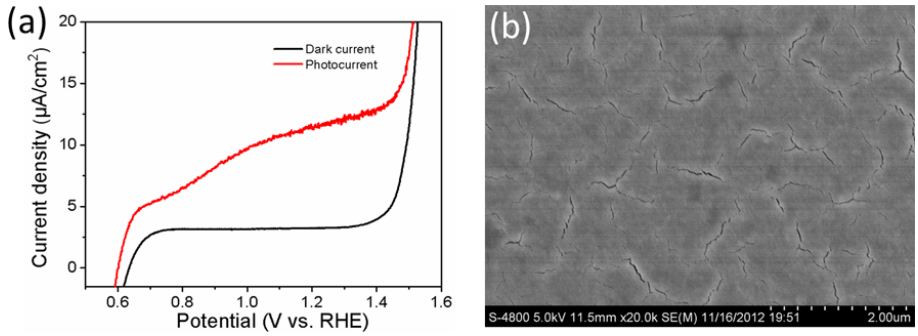

Figure S3. (a) Linear scan voltammograms of the α-Fe_2O_3/FTO, in 1 M NaOH electrolyte, in dark and under simulated AM 1.5G illumination of 100 mW/cm^2; (b) SEM image of the α-Fe_2O_3 film prepared on FTO.

Performance comparison of different Si/Fe_2O_3 photoanodes

Figure S4 shows the Linear scan voltammagrams of three different photoanodes, n-Si/α-Fe_2O_3 nanowires, p-Si/α-Fe_2O_3 nanowires and n-Si/α-Fe_2O_3 planar film. The n-Si/α-Fe_2O_3 nanowire array photoanode exhibits much better performance than the other two electrodes.

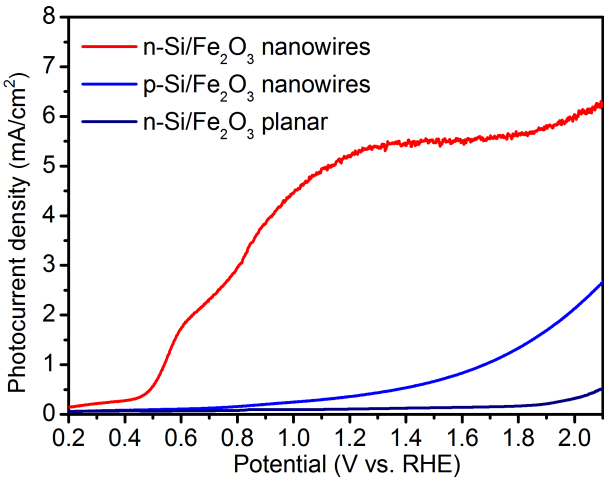

Figure S4 Linear scan voltammagrams of three different photoanodes, n-Si/α-Fe_2O_3 nanowires, p-Si/α-Fe_2O_3 nanowires and n-Si/α-Fe_2O_3 planar film.

Photoelectrochemical characterization of the SiNWs without α-Fe_2O_3 modification

Figure S5 shows the linear scan voltammograms (LSVs) of SiNWs without α-Fe_2O_3

modification. As can be seen, the SiNWs are quite unstable in the photoelectrochemical tests. In the first two LSV scans, two obvious anodic peaks, with peak current density of ca. 1.25 and 1.75 mA/cm^2, can be observed at potentials of ca. 0.2 V vs.RHE (-0.86 vs saturated calomel electrode (SCE)). The anodic peaks could be attributed to the silicon etching in the base solution (L. C. Chen et al., *J. Electrochem. Soc.* 1995, 142, 170). The absence of the anodic peaks in the LSV curves of the n-Si/α-Fe_2O_3 core/shell nanowires indicates that the SiNWs were protected by the α-Fe_2O_3 shell. After the first two scans, the photocurrent of the SiNWs quickly decreased. This could be due to damage of the SiNWs by the 1M NaOH electrolytes and the formation of insulting silicon oxides layer. After 5 LSV scans, the photocurrent quickly decreased to less than 0.1 mA/cm^2 at 1.23 V vs RHE. The later small photocurrents of SiNWs may arise from silicon oxidation and could also be because of photoelectrochemical water splitting by silicon.

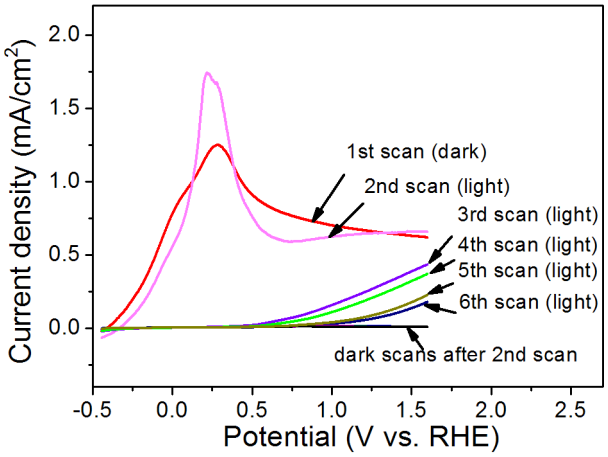

Figure S5. Linear scan voltammograms of SiNWs in 1 M NaOH electrolyte with a scan rate of 50 mV/s in dark and under simulated AM 1.5G illumination of 100 mW/cm^2.

Construction of the band diagram of the n-Si/α-Fe_2O_3/electrolyte junction

Based on the energy band data,[2,3] the schematic band diagram of the Si/α-Fe_2O_3 in various conditions are sketched in Figure S6.

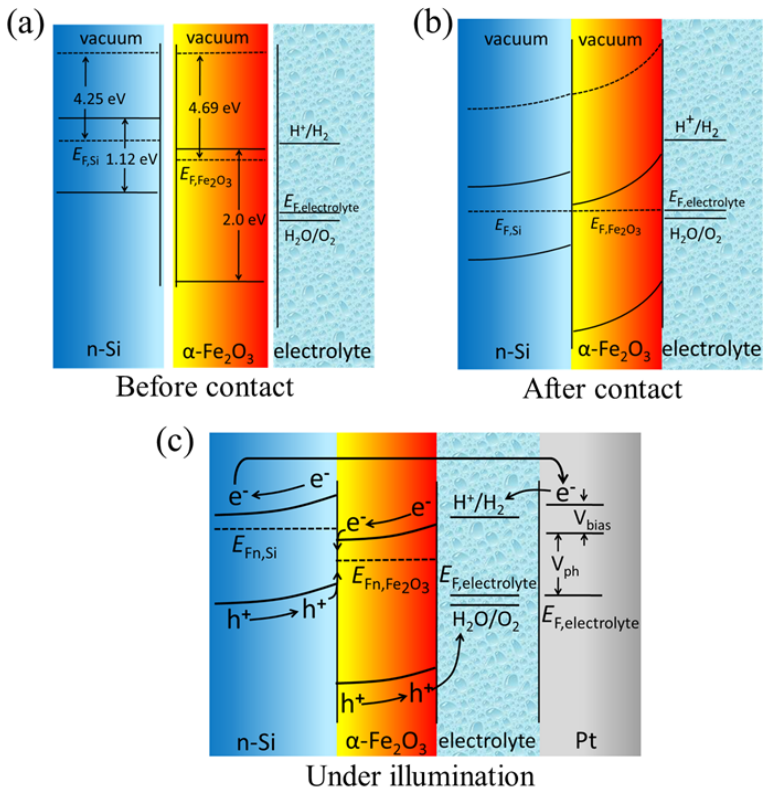

Figure S6. Energy band diagrams of Si/α-Fe_2O_3/electrolyte junction before contact (a), after contact (b) and under illumination (c).

The equilibrium of the Fermi levels of the Si, α-Fe_2O_3 and electrolyte enables the major charge carriers (electrons) in the Si and the α-Fe_2O_3 transferring to the electrolyte. As a result, a depletion layer will be formed in the Si and the α-Fe_2O_3, respectively. Since the thickness of the α-Fe_2O_3 (approximate 7.5 nm in Si/α-Fe_2O_3-20mM sample) is smaller than the calculated depletion width (16.1nm) for bulk α-Fe_2O_3 in contact with the same electrolyte, the α-Fe_2O_3 will be completely depleted from electrons and an expected accumulation layer at the region close to the Si will not exist. A resultant internal field will exist everywhere in the α-Fe_2O_3, which is critical to charge collection in the α-Fe_2O_3. This is different from previously reported n/n junctions such as Si/TiO_2 and Si/α-Fe_2O_3, where relative thick TiO_2 or α-Fe_2O_3 was used and part of the TiO_2 or α-Fe_2O_3 was in a field-free region.[4,5] Charge transfer in field-free region of α-Fe_2O_3 will be accompanied with large recombination loss due to the fact that the α-Fe_2O_3 has a

very short hole diffusion length (L_D, 2-4 nm) and short photogenerated carrier lifetime.[6,7]

Schematic energy diagram of the n-Si/α-Fe_2O_3/electrolyte junction

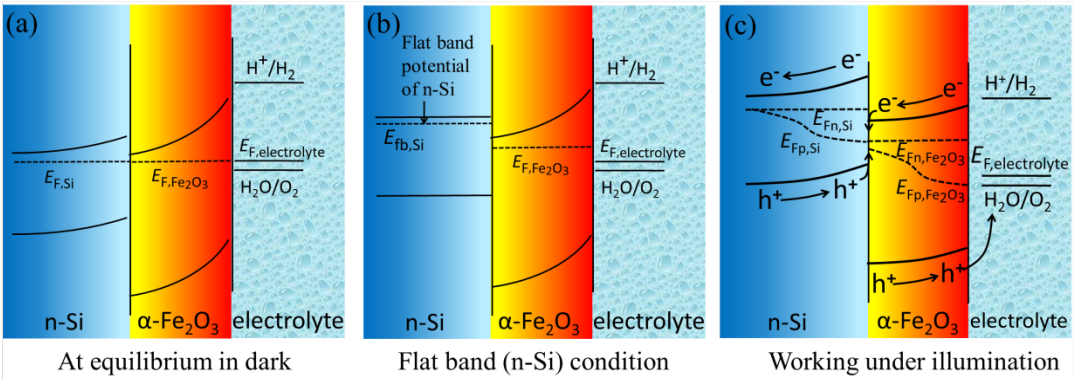

Figure S7. Schematic energy diagram of the n-Si/α-Fe_2O_3/electrolyte junction (a) at equilibrium in dark, (b) when the energy band of n-Si is flattened and (c) under illumination.

Calculation of the potential drop in the α-Fe_2O_3 shell

We assume that the α-Fe_2O_3 is so thin that it is fully depleted. The charge density distribution in the n-Si/α-Fe_2O_3, $\rho(x)$, sketched in Figure S8a, can be expressed as:

$$\rho(x) = e_0 N_{Si}\ (0 < x < w)$$

$$\rho(x) = e_0 N_{Fe2O3}\ (w < x < w + d)$$

Where w is the width of the depletion layer in the n-Si, d is the thickness of the α-Fe_2O_3, e_0 is the electron charge, N_{Si} is the density of the dopant in n-Si and N_{Fe2O3} is the density of the dopant in α-Fe_2O_3.

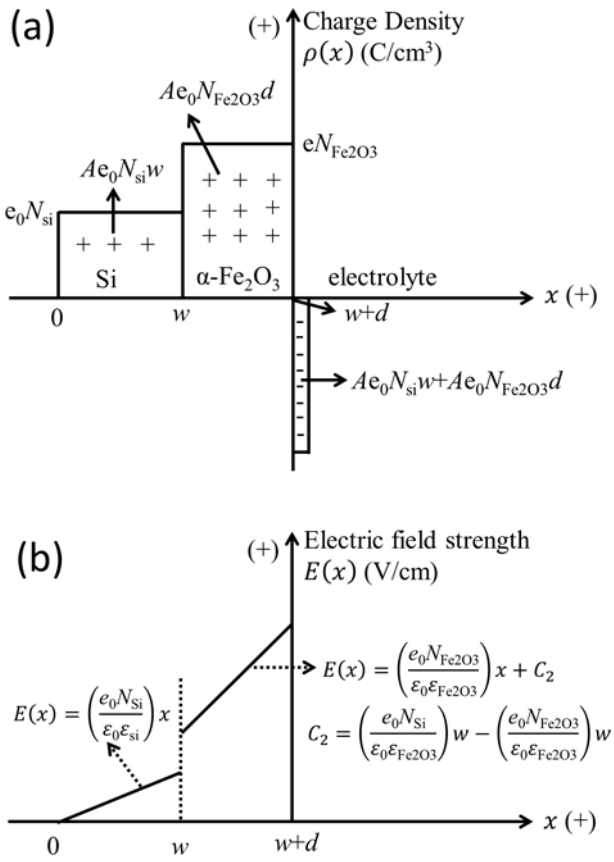

Figure S8. (a) Charge Density and (b) electric field strength distributions in the n-Si/α-Fe_2O_3/electrolyte junction

According the Poisson equation, the potential distribution, $V(x)$, is expressed as:

$$\frac{\partial^2 V(x)}{\partial x^2} = -\frac{\rho(x)}{\varepsilon_0 \varepsilon_s} \quad [\varepsilon_s = \varepsilon_{Si}\ (0 < x < w),\ \varepsilon_s = \varepsilon_{Fe2O3}\ (w < x < w + d)]$$

Where ε_s is the relative permittivity of the material and ε_0 is the vacuum permittivity. The electric field strength, $E(x)$, is expressed as:

$$E(x) = -\frac{\partial V(x)}{\partial x}$$

By integrating the Poisson equation with x, we obtain

$$E(x) = \left(\frac{e_0 N_{Si}}{\varepsilon_0 \varepsilon_{si}}\right) x + C_1 (0 < x < w)$$

$$E(x) = \left(\frac{e_0 N_{Fe2O3}}{\varepsilon_0 \varepsilon_{Fe2O3}}\right) x + C_2\ (w < x < w + d)$$

We take the boundary condition into account. At x=0, it is assumed that $E(x)$=0. Then, $C_1 = 0$. At x=w, there is $\varepsilon_{si} E_{si}(w) = \varepsilon_{Fe2O3} E_{Fe2O3}(w)$. We obtain

$$C_2 = \left(\frac{e_0 N_{\mathrm{Si}}}{\varepsilon_0 \varepsilon_{\mathrm{Fe2O3}}}\right) w - \left(\frac{e_0 N_{\mathrm{Fe2O3}}}{\varepsilon_0 \varepsilon_{\mathrm{Fe2O3}}}\right) w$$

Then, integrating the electric field strength $E(x)$ (illustrated in Figure S8b) within the α-Fe_2O_3, i.e., from $x=w$ to $x=w+d$, yields a quantified expression of the potential drop in the α-Fe_2O_3, V_{Fe2O3}.

$$V_{Fe2O3} = \left(\frac{e_0 N_{\mathrm{Fe2O3}}}{2\varepsilon_0 \varepsilon_{\mathrm{Fe2O3}}}\right) d^2 + \left(\frac{e_0 N_{\mathrm{si}} w}{\varepsilon_0 \varepsilon_{\mathrm{Fe2O3}}}\right) d$$

It can be seen that the first term in the expression is in the same form as the potential drop in the depletion layer of a single semiconductor in contact with an electrolyte, which can be assigned to the contribution of the positive charge in the depleted α-Fe_2O_3 and the corresponding negative charge transferred from the α-Fe_2O_3 to the electrolyte. The second term takes the form of the potential drop between the two plates of a parallel plate capacitor and can be attributed to the contribution of the positive charge in the depletion layer of the n-Si and the corresponding negative charge transferred from the n-Si to the electrolyte.

Impact of α-Fe_2O_3 thickness on energy diagram of n-Si/α-Fe_2O_3/electrolyte junction

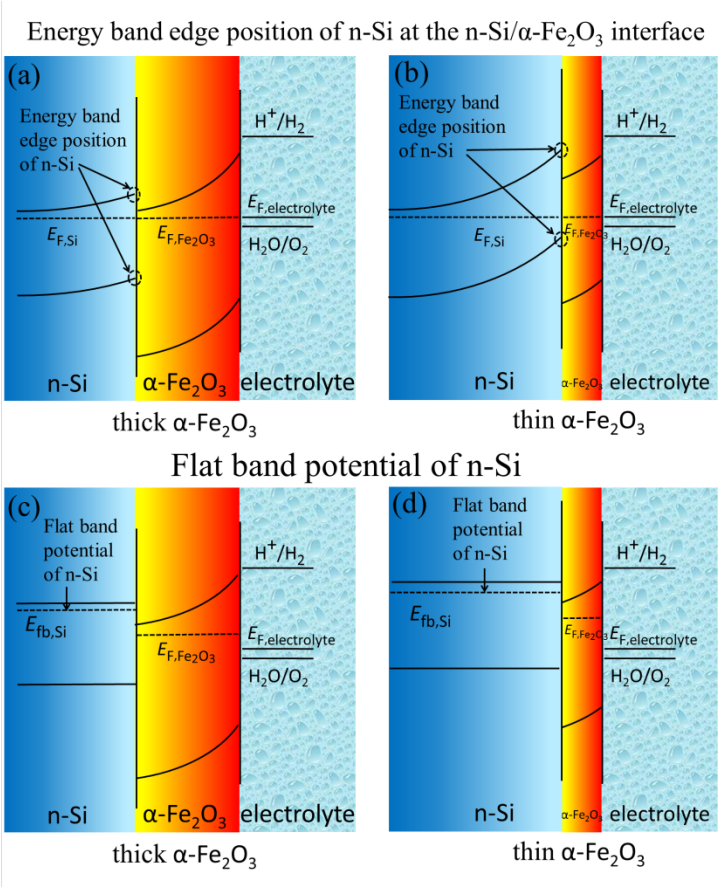

Figure S9. Energy band edge position of n-Si at the n-Si/α-Fe_2O_3 interface when (a) thick α-Fe_2O_3 and (b) thin α-Fe_2O_3 is used; n-Si/α-Fe_2O_3/electrolyte junction in dark when the energy band of n-Si is flattened, when (c) thick α-Fe_2O_3 and (d) thin α-Fe_2O_3 is used.

Stability of the n-Si/α-Fe_2O_3 core/shell nanowire arrays

Figure S10 shows the photocurrent-time curve of an n-Si/α-Fe_2O_3-20mM sample. After the initial quick decrease, the photocurrent reached a relatively steady state. The sample exhibited good stability, retaining a photocurrent larger than 1.7 mA/cm^2 after 3 hours.

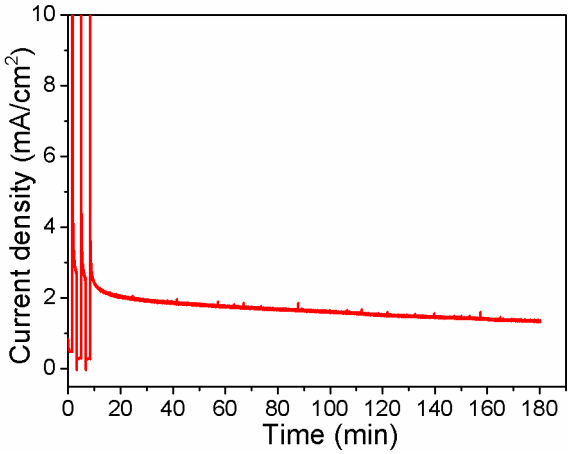

Figure S10. Long-term stability test of 180 min on the n-Si/α-Fe_2O_3-20mM sample, under simulated AM 1.5G illumination of 100 mW/cm^2.

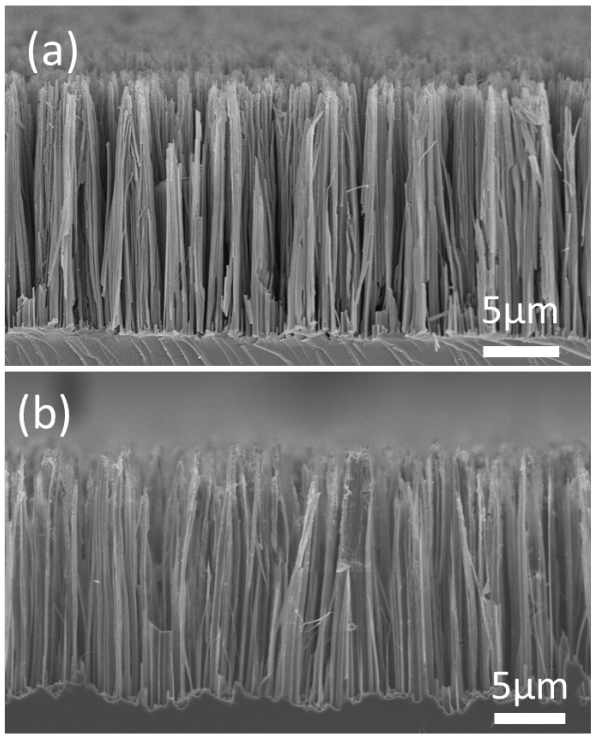

Figure S11. SEM images of the n-Si/α-Fe_2O_3-20mM (a) before and (b) after stability test for 3 hours at a fixed potential of 1.6 V vs RHE, under simulated AM 1.5G illumination of 100 mW/cm^2.

The morphology change of the sample after long-term test was analyzed by SEM. Figure S11 compares the morphology of an n-Si/α-Fe_2O_3-20mM sample before and after long-term test. After 3 hours measurement under illumination, the morphology of the n-Si/α-Fe_2O_3 nanowire arrays does not change significantly. Some broken nanowires

were observed after 3 hours measurement, which may be due to the corrosion of the inner Si core by the strong alkaline electrolyte (1 M NaOH) penetrating from places where the Si is not perfectly protected by the α-Fe_2O_3.

Discussions on the mass transport in the n-Si/α-Fe_2O_3 core/shell nanowires

Due to the fact that the mass transport in an electrochemical cell, i.e. the transport of the redox species (OH^- in the 1 M NaOH in our cell) from the bulk in the electrolyte to the electrode surface, may influence the magnitude of current measured in linear scan voltammetry, [8] we performed linear scan voltammetry measurements with different potential scan rates in electrolyte with different magnetic stirring. Figure S12a shows the LSV curves of the n-Si/α-Fe_2O_3-20mM with scan rates of 50 mv/s, 20 mv/s and 10 mv/s, measured in electrolyte with moderate magnetic stirring. As can be seen, the onset potentials remain almost identical as the potential scan rates were decreased, however the photocurrent decreases with the decreasing scan rates. Also, it can be seen that the dark currents measured under various scan rates are all very small relative to the photocurrents, suggesting that the behavior of the photocurrent under different scan rates is not due to some capacitive currents which could result from charging/discharging the depletion layer and/or iron adsorbing/desorbing in the double layer and are proportional to the scan rates.

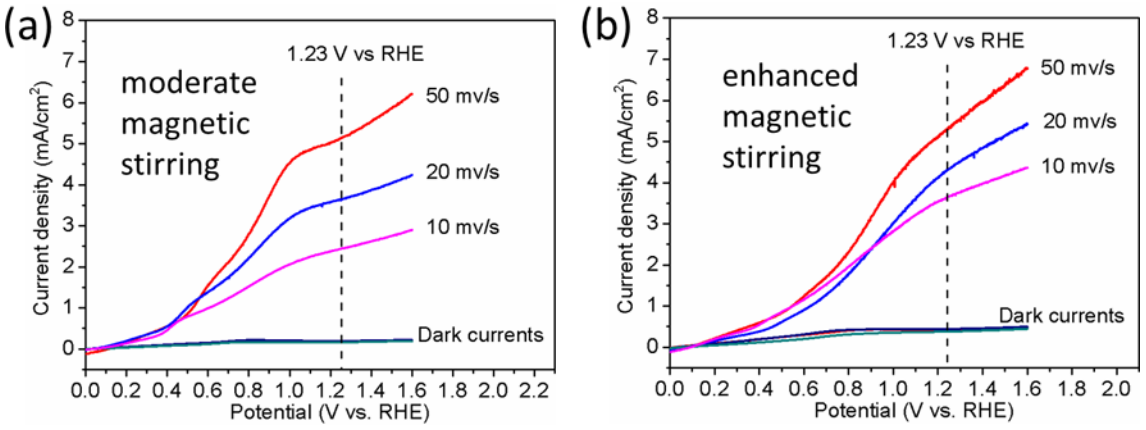

Figure S11. Linear scan voltammograms of n-Si/α-Fe_2O_3-20mM samples with potential scan rates of

50 mV/s, 20 mV/s and 10 mV/s, in 1 M NaOH electrolyte (a) with moderate magnetic stirring and (b) with enhanced magnetic stirring, under simulated AM 1.5G illumination of 100 mW/cm^2.

When faster-rate magnetic stirring was used to enhance the mass transport by enhancing the convection of the electrolyte, the influence of the scan rate on the photocurrent magnitude could be minimized, as can be seen in Figure S12b. This clearly demonstrates that the mass transport is limiting the photocurrent, even though we used magnetic stirring to enhance the mass transport by forcing the convection of the electrolyte. The influence of the potential scan rate on the current magnitude record from liner scan voltammetry in a mass-transport-limiting cell could be rationalized by the time to record the current and the depletion of the redox species at the electrode surface as well as the size of the diffusion layer. [8]

The inefficient mass transport is possibly related with the unique architecture of the nanowire arrays. Previous research has revealed that the convective mass transport (forced by the magnetic stirring) only effect within a few micrometer from the top of the microwire array to the internal. [9] In the internal void volume in the array, the mass transport is mainly forced by diffusion (movement of a reactant under the influence of its concentration gradient), which is inefficient. The “steady-state” photocurrents measured in the Photocurrent-Time curves in the stability tests may also be limited by the inefficient mass transport, i.e., the supply of the redox species from the bulk in the cell to the electrode surface.

References

[1] Peng, K. Q.; Wu, Y.; Fang, H.; Zhong, X. Y.; Xu, Y.; Zhu, J. *Angew. Chem., Int. Ed.* **2005,** 44, 2737-2742.

[2] Novikov, A. *Solid-State Electron.* **2010,** 54, 8-13.

[3] Xu, Y.; Schoonen, M. A. A. *Am. Mineral.* **2000,** 85, 543-556.

[4] Hwang, Y. J.; Boukai, A.; Yang, P. *Nano Lett.* **2009,** 9, 410-415.

[5] Mayer, M. T.; Du, C.; Wang, D. *J. Am. Chem. Soc.* **2012,** 134, 12406-12409.

[6] Cherepy, N. J.; Liston, D. B.; Lovejoy, J. A.; Deng, H. M.; Zhang, J. Z. *J. Phys. Chem. B* **1998,** 102, 770-776.

[7] Kennedy, J. H.; Frese, K. W. *J. Electrochem. Soc.* **1978,** 125, 709-714.

[8]Bard, A. J.; Faulkner, L. R. Chapter 6. Potential Sweep Methods. In *Electrochemical Methods: Fundamentals and Applications,* 2nd ed.; John Wiley & Sons, Inc.: New York, **2000**; pp 226-260.

[9] Xiang, C. X.; Meng, A. C.; Lewis, N. S. *Proc. Natl. Acad. Sci. U.S.A.* **2012**, 109, 15622-15627.